Quasi Steady-State Modeling and Characterization of Diffusion-Controlled Dissolution from Polydisperse Spheroidal Particles, I: Modeling

Yanxing Wang^{1,*}, Hui Wan², Rusitan Refuaiti¹, Tie Wei³, and Fangjun Shu¹,

¹Department of Mechanical and Aerospace Engineering, New Mexico State University, Las Cruces, NM 88003, USA ²Department of Mechanical and Aerospace Engineering, University of Colorado, Colorado Springs, CO 80918, USA ³Department of Mechanical Engineering, New Mexico Institute of Mining and Technology, Socorro, NM 87801, USA

A quasi steady-state model (QSM) for accurately predicting the detailed diffusion-dominated dissolution process of polydisperse spheroidal (prolate, oblate, and spherical) particle systems with a broad range of distributions of particle size and aspect ratio has been developed. A rigorous, mathematics-based QSM of the dissolution of single spheroidal particles has been incorporated into the well-established framework of polydisperse dissolution models based on the assumption of uniform bulk concentration. Validation against experimental results shows that this model can accurately predict the increase in bulk concentration of polydisperse systems with various particle sizes and shape parameters. A series of representative instances involving the dissolution of polydisperse felodipine particles at various concentration ratios is used to demonstrate the model's effectiveness, rendering it a valuable tool for understanding and managing complex systems with diverse particle characteristics.

Introduction

The modeling and characterization of dissolution processes in multiple-solid-particle systems is of great importance to many scientific and industrial applications, from traditional drug delivery [1] and metal ore heap leaching [2] to emerging renewable biomass energy [3] and dissolvable microrobots [4]. A full understanding of dissolution kinetics not only enables accurate predictions of the variations of solution concentration and particle sizes, but also carries crucial implications for controlling and optimizing the dissolution process. For example, the dissolution characteristics of drug particles play a pivotal role in determining and manipulating drug release and the bioavailability of active pharmaceutical ingredients. Hence, it is vital to understand the underlying physical and chemical processes involved [5].

One of the limiting factors for particle dissolution rate is the transport of dissolved molecules from the particle surface to the surrounding fluid, and this process relies on both molecular diffusion and the hydrodynamics around the particle. In some applications, such as drug dissolution in the gastrointestinal tract, the particle sizes range from a few microns to hundreds of microns [6, 7]. For such small particles, hydrodynamic effect is relatively weak and molecular diffusion plays a dominant role in mass transfer [8]. To date, a large number of diffusion-dominated dissolution models have been developed and broadly used in various areas [9]. Among these models, the most widely used models are the Fick's-first-law-based Noyes-Whitney Model and its modifications [5, 10-19]. The basic idea of these models is to establish a linear relationship between the particle dissolution rate and the difference in concentration between particle surface and bulk fluid. They typically incorporate a parameter known as diffusion layer thickness, which is based on the recognition that a layer of high concentration fluid exists adjacent to the particle surface [9, 16]. For spherical particles, the diffusion layer thickness is considered to be close to the particle radius.

^{*}yxwang@nmsu.edu

These models have been shown to accurately predict the entire dissolution process of spherical particles, but they are generally empirical or semi-empirical, lacking rigorous mathematical proof, and having limited applicability. Beyond the empirical and semi-empirical models, some mathematical models built on solutions of the diffusion equation of a spherical particle have been proposed, such as the infinite-domain model [20], the finite-domain model [21], and the quasi-steady-state model [21, 22]. Wang et al.[21] conducted a critical examination of the accuracy and efficiency of these models. They found that a relatively simple "quasi steady-state" model (QSM) predicts both the increase in bulk concentration and the surface flux with a high level of accuracy beyond a short initial transient period. QSM thus can be used as the basis for developing more sophisticated dissolution models.

Currently, the major challenges in modeling the dissolution processes of real particle systems involve the treatment of wide distributions of particle sizes and geometries. In practical applications, particle sizes typically vary within a range, rather than being uniform [23]. Particles of different sizes have different dissolution rates. To the best of our knowledge, the earliest polydisperse model was developed by Higuchi and Hiestand for spherical particles[22]. Their model assumes that the diffusion layer thicknesses are always equal to the particle radius and uses the Noyes-Whitney equation to calculate the dissolution rate of each individual particle. However, they only considered the bulk concentration to be constant, leading to independent dissolution of all the particles. Therefore, this model is not a real polydisperse model. Based on Higuchi and Hiestand's model[22], Hintz and Johnson [16] proposed a new model, in which they calculated the bulk concentration by summing the numbers of molecules dissolving from every particle and dividing it by the total container volume. In this model, the diffusion layer thickness, δ , depends on the particle size. For particles with a radius smaller than 30 μ m, δ is set equal to the particle radius, while for all larger particles, δ is fixed at 30 µm. This model has become the most popular tool for investigating the polydisperse dissolution mechanisms, and has been used broadly to date [24]. The advantage of the Hintz and Johnson's model is that it avoids the complexity of solving the diffusion equation around each particle, and describes the dissolution rate through a simple linear expression involving the surface area and the difference between bulk concentration and saturation concentration. However, because species transport around each particle is still not well understood, the diffusion layer thickness δ still needs to be modeled. Taking advantage of the easy form of the solution of the OSM, Wang et al. [25] developed a "hierarchical" model to predict the detailed dissolution process from polydisperse collections of spherical particles of various sizes. Since Wang et al.'s model is based on an analytical solution to the diffusional transport equation for individual particles, it provides more physical insight, including the spatial distribution of dissolved species around each particle. The basic idea of this model provides an important direction for developing dissolution models for polydisperse non-spherical particles.

In nature, however, and in practical applications, more than 70% of solid particles are not regularly spherical, and have a wide range of aspect ratio from O(0.1) to O(10) [26, 27]. Morphology has been identified as a key factor influencing dissolution[1, 26, 27]; the assumption of spherical particles may be one of the dominant sources of error in quantifying the dissolution process. Wang et al. [28] have extended the QSM for spherical particles to include prolate and oblate spheroidal particles. The new model is based on the analytical solutions of the steady-state diffusion equation in spheroidal coordinate systems. According to the spatial distribution of molar concentration in the surrounding fluid, detailed dissolution processes, such as the molar flux of dissolved substances and the regression rate of the particle surface, can be obtained.

A robust and straightforward mathematical model capable of comprehensively addressing the intricate dissolution process of a polydisperse particle system with diverse sizes and geometries is still lacking, and the dissolution characteristics of such particle systems are still not well understood. This severely impedes the optimization and control of particle dissolution in various applications. In this paper, we develop a dissolution model for polydisperse spheroidal particles with distributions of both size and aspect ratio, based on the QSM for spheroidal particles [28] and the polydisperse model for spherical particles [25]. The aspect ratio covers a wide range of particle shapes from prolate to oblate spheroidal particles. The present study

proposes a physics-based, easy to use, and accurate tool for research on the dissolution of a wide range of particle systems, and offers insights into the dissolution kinetics of complex systems. This model is intended to establish a foundation for future development of more intricate dissolution models that take into account the hydrodynamics around the particles in such systems.

Mathematical model formulations

(a) Single or monodisperse particle modeling

In this study, the term "monodisperse" is used to denote a system in which all particles have the same size and shape, and "polydisperse" is used to denote a system in which the particles have either various sizes or various shapes or both. In terms of modeling strategy, the monodisperse model is the same as the single particle model. For the polydisperse dissolution model, we build a collection of particles of different sizes and shapes, in which the dissolution of each particle is partially described by a single particle dissolution model and is coordinated by the polydisperse model. In this study we focus on spheroidal shapes from prolate to spheric and then to oblate. The QSM for a single prolate or oblate spheroidal particle proposed by Wang et al.[21] are used to model the dissolution of each particle.

The surface of a spheroidal particle is described by

$$\frac{x^2 + y^2}{a_n^2} + \frac{z^2}{b_n^2} = 1\tag{1}$$

where x, y, and z are Cartesian coordinates, a_p is the equatorial radius, and b_p is the polar radius. The aspect ratio is defined as,

$$\Lambda = a_p / b_p \tag{2}$$

When $\Lambda > 1$, the particle shape is oblate spheroidal, when $\Lambda < 1$, the shape is prolate spheroidal, and when $\Lambda = 1$, the shape is spherical.

At the particle surface, the concentration of dissolved substance is the saturated concentration, which is constant.

$$C = C_{\rm c} \tag{3}$$

where C(x, y, z) (mol/volume) is the molar concentration of dissolved substance, and C_s is the saturated concentration.

The molar flux of dissolved substance from the particle surface to the surrounding liquid, $N_S^{"}$ (mol/areatime), is defined as

$$N_{\mathsf{S}}^{"} = -D_{m}\vec{n} \cdot \nabla C|_{\mathsf{S}} \tag{4}$$

where D_m (area/time) is the diffusion coefficient for the dissolved substance in the fluid, and \vec{n} is a unit normal vector pointing outwards to the ambient fluid. The particle surface regresses with time as the particle loses mass from its surface,

$$\frac{dR_n}{dt} = -N_S^" v_m \tag{5}$$

where R_n is the surface coordinate in the direction normal to the particle surface, and v_m (volume/mol) is the specific volume of the particle.

For a given particle, the dissolution also depends on the container volume, which confines the dissolved substance within the container. From the initial particle volume (V_{p0}) and container volume (V_c), the initial solid particle concentration, C_{p0} (mol/volume), is calculated as

$$C_{p0} \equiv \frac{v_{p0}}{v_m V_c} \tag{6}$$

In the calculation, either V_c or C_{p0} can be used to specify the container volume.

According to Wang et al. [28], for each prolate or oblate particle, the release rate through the particle surface, which is denoted by N'_s (mol/time), is,

$$N_{\rm S}' = -4\pi A D_m \Omega \tag{7}$$

where A and Ω are coefficients related to the geometry of the particle and the profile of the substance concentration. For a prolate spheroid,

$$A = \frac{C_S - C_{\infty}}{\ln\left(\frac{b_p + a_p - \Omega}{b_n + a_n + \Omega}\right)} \tag{8}$$

$$\Omega = \sqrt{b_p^2 - a_p^2} \tag{9}$$

and for an oblate spheroid,

$$A = \frac{C_S - C_{\infty}}{\arctan(b_p/\Omega) - \pi/2} \tag{10}$$

$$\Omega = \sqrt{a_p^2 - b_p^2} \tag{11}$$

where C_{∞} is the concentration of dissolved substance at infinity. C_{∞} is related to the bulk concentration C_b via the container size [21].

When $a_n = b_n$, Eqn. (7) collapses into the expression for spherical particles, which is written as [21],

$$N_{\rm S}' = -4\pi R D_m (C_{\rm S} - C_{\infty}) \tag{12}$$

Equations (7) and (12) describe the release rates of spheroidal particles of different aspect ratios.

During dissolution the particle size gradually decreases. It is shown in Wang et al.[28] that the aspect ratios of the prolate and oblate particles, $\Lambda = a_p(t)/b_p(t)$, do not change over time. It is more convenient to use the radius of a spherical particle of the same volume to represent the size of non-spherical particles. The size of all particles can be uniformly expressed by the equivalent spherical radius,

$$R = \left(a_p^2 b_p\right)^{1/3} \tag{13}$$

Then the reduction rate of R can be calculated from the release rate at the surfaces of both spherical and non-spherical particles,

$$\frac{dR}{dt} = \frac{N_S' v_m}{4\pi R^2} \tag{14}$$

An alternative to calculate N_S' is to utilize the idea that the release of dissolved substance is realized by the diffusion of the substance through a diffusion layer thickness at the particle surface.

$$N_S' = -4\pi R^2 D_m \frac{(C_S - C_b)}{\delta(t)} \tag{15}$$

where $\delta(t)$ is the diffusion layer thickness defined based on the equivalent spherical particle radius. $\delta(t)$ is obtained from the QSM for spherical [21] or non-spherical particles [28].

(b) Polydisperse particle modeling

Currently, there are two major strategies for building models of polydisperse particle dissolution. In the first, proposed by Hintz and Johnson [16], the dissolution rate of each particle is calculated by the difference of substance concentration between the particle surface and the bulk fluid over a diffusion layer. In the second, proposed by Wang et al. [25], the dissolution of each particle is described by the QSM within a finite-sized container. These two strategies share a common assumption that the solution is perfectly mixed and the bulk concentration of dissolved substance is uniform throughout. The bulk concentration is "felt" by every particle and is used to calculate the dissolution rate of every particle. When the diffusion layer thickness in the Hintz and Johnson's model is obtained from the QSM, the two strategies essentially become the same. Both strategies are currently used only for spherical or near-spherical particles, due to the lack of a dissolution model for non-spherical particles. In this study, we take advantage of the QSM for prolate and oblate particles and extend the aforementioned polydisperse models to those for systems with various particle sizes and shapes. The two strategies for polydisperse dissolution are introduced in more detail below.

Sub-container model

Here we extend the Wang et al. [25] model for spherical particles to a system with a wide range of particle size and aspect ratio. Figure 1 shows the physical model. In a container holding n particles, the container is broken down into as many separate sub-containers as the number of particles, and each particle is assigned a sub-container. We assume that the sub-containers are spheroidal, with every particle positioned at the center of its respective sub-container. The substance released by a particle remains confined within its corresponding sub-container. The linkage among the particles is established by keeping the bulk concentration in each sub-container the same as the bulk concentration in the whole container. The bulk concentration in the container is,

$$C_b = \frac{N}{V_c} = \frac{N_1 + N_2 + \dots + N_i + \dots + N_n}{V_{c,1} + V_{c,2} + \dots + V_{c,i} + \dots + V_{c,n}} = \frac{\sum_{1}^{n} N_i}{\sum_{1}^{n} V_{c,i}}$$
(16)

where $N_1, N_2, ..., N_n$ are the amounts of substance released from every particle, N is the total amount of substance released from all particles, and $V_{c,1}, V_{c,2}, ..., V_{c,n}$ are the volume of every sub-container, with the sum of the sub-container volumes being equal to the volume of the whole container V_c . The amount of substance released from the *i*-th particle is acquired by integrating the surface release rate of the particle over time,

$$N_i(t) = \int_0^t N'_{S,i}(\tau)d\tau \tag{17}$$

where $N'_{S,i}(\tau)$ is calculated from Eqns. (7) and (12). The bulk concentration in every sub-container is calculated by,

$$C_{b,1} = \frac{N_1}{V_{c,1}}, C_{b,2} = \frac{N_2}{V_{c,2}}, ..., C_{b,i} = \frac{N_i}{V_{c,i}}, ..., C_{b,n} = \frac{N_n}{V_{c,n}}$$
(18)

To keep $C_{b,i}(t)$ always equal to $C_b(t)$, the volume of each sub-container is adjusted dynamically at every moment.

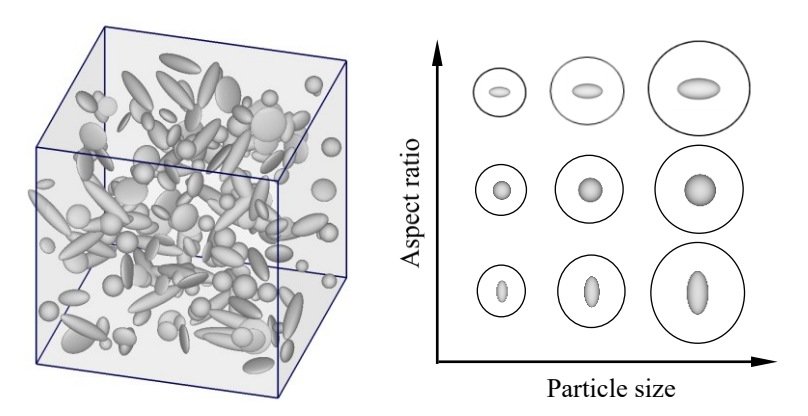


Figure 1. Illustration of sub-container model for dissolution from a polydisperse collection of spheroidal particles of a variety of particle sizes and aspect ratios. The dissolution of each particle is described by the QSM of a single particle in a sub-container.

In systems comprising spherical particles, this model provides a prediction of the dissolution process that is consistent with experimental measurement [25]. This model serves as the basic tool for analyzing the polydisperse dissolution in this study.

Diffusion layer model

In the Hintz and Johnson diffusion layer model [16], a Noyes-Whitney type expression [29] is applied to describe the dissolution of the particles, and a diffusion layer thickness is used to calculate the dissolution rate,

$$N'_{S,i} = -A_{p,i}D_m \frac{(C_s - C_b)}{\delta_i(t)} \tag{19}$$

where $A_{p,i}$ is the surface area and $\delta_i(t)$ is the diffusion layer thickness of the *i*-th particle. Here the bulk concentration C_b is also calculated by Eqn. (16). The diffusion layer thickness is obtained through mathematical models or experimental measurements. Prior to the emergence of rigorous mathematical models such as FDM and QSM [21], the determination of the diffusion layer thickness played a pivotal role in a number of modeling strategies [9].

It was found that the QSM accurately predicts both the time-varying bulk concentration and the surface flux beyond a short initial transient period [21]. A reasonable way to take advantage of the aforementioned sub-container model is to assign each particle a sub-container, and then use the QSM to acquire the time dependent diffusion layer thickness. With this treatment, the diffusion layer model is exactly the same as the sub-container model. A simplified version uses the QSM for a single particle to develop a correlation of diffusion layer thickness as a function of particle size and geometry and other determining factors, and then incorporate the correlation into the polydisperse model of dissolution rate shown by Eqn. (19). Obviously, both methods of the diffusion layer model will offer the same level of accuracy as the sub-container model.

(c) Population Balance Modeling

In polydisperse systems, it is convenient to use the temporal evolution of a probability distribution function (PDF) with respect to the equivalent spherical radius (R) and aspect ratio (Λ) to describe the

statistical average state of the particles. Here we define the volumetric probability distribution function of particle radius and aspect ratio as

$$P_{R,\Lambda}^{\nu}(R,\Lambda,t)\delta R\delta \Lambda \equiv \frac{\delta(V_p(t))_{R\to R+\delta R,\Lambda\to\Lambda+\delta\Lambda}}{V_p(t)} \tag{20}$$

and

$$\int_{R_{min}}^{R_{max}} \int_{\Lambda_{min}}^{\Lambda_{max}} P_{R,\Lambda}^{\nu}(R,\Lambda,t) dR d\Lambda = 1$$
 (21)

where $P^v_{R,\Lambda}(R,\Lambda,t)$ is the volumetric PDF of particle radius and aspect ratio at time t, $\delta \left(V_p(t)\right)_{R\to R+\delta R,\Lambda\to\Lambda+\delta\Lambda}$ is the volume of particles with radius between R and $R+\delta R$ and aspect ratio between Λ and $\Lambda+\delta\Lambda$, $V_p(t)$ is the total particle volume, R_{min} and R_{max} are the minimum and maximum particle radii, and Λ_{min} and Λ_{max} are the minimum and maximum particle aspect ratios, respectively.

Considering the width of the range of Λ for prolate spheroids ($\Lambda < 1$) is much smaller than that for oblate spheroids ($\Lambda > 1$), we further create the PDF using the Taylor shape parameter instead of aspect ratio, following the description of droplet morphology [30]. The Taylor shape parameter is defined as,

$$D = \frac{a_p - b_p}{a_p + b_p} \tag{22}$$

The relationship between D and Λ is,

$$D = \frac{\Lambda - 1}{\Lambda + 1} \tag{23}$$

The corresponding volumetric PDF with respect to R and D is written as,

$$P_{R,D}^{\nu}(R,D,t)\delta R\delta D \equiv \frac{\delta(V_p(t))_{R\to R+\delta R,D\to D+\delta D}}{V_p(t)}$$
(24)

and

$$\int_{R_{min}}^{R_{max}} \int_{D_{min}}^{D_{max}} P_{R,D}^{v}(R,D,t) dR dD = 1$$
 (25)

where $\delta(V_p(t))_{R\to R+\delta R, D\to D+\delta D}$ is the particle volume in the ranges from R to $R+\delta R$ and from D to $D+\delta D$.

The population balance model (PBM) presenting the partial differential equation of the PDF of time and particle radius has been broadly used in the study of solid particle dissolution[31-33]. By studying the time rate of change of particle volume in a control volume in the space of *R* and *D*, the following population balance equation can be easily obtained,

$$\frac{\partial}{\partial t} \left(P_{R,D}^{\nu} V_p \right) = -\frac{\partial}{\partial R} \left(P_{R,D}^{\nu} V_p \frac{dR}{dt} \right) - \frac{\partial}{\partial D} \left(P_{R,D}^{\nu} V_p \frac{dD}{dt} \right) \tag{26}$$

It is shown in Wang et al. [28] that the aspect ratios of prolate and oblate particles do not change over time, so $\frac{dD}{dt} = 0$ and Eqn. (26) reduces to,

$$\frac{\partial}{\partial t} \left(P_{R,D}^{\nu} V_p \right) = -\frac{\partial}{\partial R} \left(P_{R,D}^{\nu} V_p \frac{dR}{dt} \right) \tag{27}$$

(d) Volumetric PDF in Logarithm Scale of Particle Radius

In fields such as pharmacology and crystallography, the log-normal distribution has been used for a long time to describe the size distribution of particles; the particle distribution is described as a normal or Gaussian function on a logarithm scale of particle size [34, 35]. Here, we define the volumetric PDF of particle size with respect to the logarithm of equivalent spherical particle radius as,

$$P_{logR,D}^{v}(logR,D,t)\delta(logR)\delta D \equiv \frac{\delta(V_{p}(t))_{logR\to logR+\delta(logR),D\to D+\delta D}}{V_{p}(t)}$$
(28)

and

$$\int_{logR_{min}}^{logR_{max}} \int_{D_{min}}^{D_{max}} P_{logR,D}^{v}(logR,D,t) d(logR) dD = 1$$
(29)

where $\delta(V_p(t))_{logR \to logR + \delta(logR), D \to D + \delta D}$ is the particle volume with a logarithm of radius between logR and $logR + \delta(logR)$ and Taylor parameter between D and $D + \delta D$.

Here we consider the simplest case, in which the dependence of $P^{v}_{logR,D}$ on logR is decoupled from that on D and the dependence on logR follows the log-normal distribution. Then volumetric PDF can be defined separately for logR and D, which are denoted by $P^{v}_{logR}(logR,t)$ and $P^{v}_{D}(D,t)$, respectively,

$$P_{logR}^{v}(logR,t) \equiv \int_{D_{min}}^{D_{max}} P_{logR,D}^{v}(logR,D,t)dD$$
(30)

$$P_D^{\nu}(D,t) \equiv \int_{logR_{min}}^{logR_{max}} P_{logR,D}^{\nu}(logR,D,t)d(logR)$$
(31)

and

$$P_{logR,D}^{v}(logR,D,t) = P_{logR}^{v}(logR,t)P_{D}^{v}(D,t)$$
(32)

A volumetric PDF with a log-normal distribution with respect to logR at t=0 reads

$$P_{logR,0}^{v}(logR) = \frac{1}{\sqrt{2\pi\sigma^2}} exp\left[-\frac{(logR-logR^*)^2}{2\sigma^2}\right]$$
(33)

where σ is the standard deviation of the distribution, and R^* is the particle radius at which the maximum $P_{logR,0}^{v}$ is reached.

(e) Implementation of Polydisperse Dissolution Model

Given an initial $P_{logR,D,0}^{v}$ as a function of logR and D, $P_{logR}^{v}(t)$ evolves from $P_{logR,D,0}^{v}$ with time as a consequence of variations of the size and shape of every particle. To simplify the problem, we assume that at t = 0, $P_{logR,D,0}^{v}$ follows the log-normal distribution with respect to logR for any D and is uniform over D from D_{min} to D_{max} for any logR,

$$P_{logR,D,0}^{v}(logR,D) = P_{logR,0}^{v}(logR)/(D_{max} - D_{min})$$
(34)

and $P_{logR,0}^{v}$ is described by a log-normal function given by Eqn. (33). $P_{logR,D,0}^{v}$ is finally written as,

$$P_{logR,D,0}^{v}(logR,D) = \frac{1}{\sqrt{2\pi\sigma^2}} exp\left[-\frac{(logR-logR^*)^2}{2\sigma^2}\right] / (D_{max} - D_{min})$$
 (35)

To implement the polydisperse model, the initial volumetric PDF of particle sizes and shapes, that is, $P_{logR,D,0}^{v}$, has to be discretized into a number of bins with respect to logR and D. An easy way is to

decompose the space of logR and D into $n_{logR} \times n_D$ bins, and the bins have uniform bin width in logR and D, as shown in Fig. 2. The bin widths are given as

$$\Delta_{logR} = (logR_{max} - logR_{min})/(n_{logR} - 1)$$
(36)

$$\Delta_D = (D_{max} - D_{min})/(n_D - 1) \tag{37}$$

where n_{logR} and n_D are the numbers of bins in logR and D, respectively. We assume that in each bin all the particles have the same values of logR and D. The number of particles in bin (i, j) is (see Fig. 2),

$$n_{p,(i,j)} = \frac{P_{logR,D,0}^{\nu} \Delta_{logR} \Delta_{D} V_{p,0}}{\frac{4}{3} \pi R^{3}}$$
 (38)

where $V_{p,0}$ is prespecified total volume of particles. In the dissolution process, $n_{p,(i,j)}$ does not change with time, yet the bin widths, Δ_{logR} and Δ_D change due to the reduction of particle sizes in the bins.

Based on R^* , we define a dissolution time scale for a polydisperse system, τ_{diss} , which is the time scale required for a spherical particle with radius R^* to fully dissolve at zero bulk concentration,

$$\tau_{diss} = \frac{R^{*2}}{2\nu_m C_s D_m} \tag{39}$$

 τ_{diss} will be used to normalize time t in the analysis.

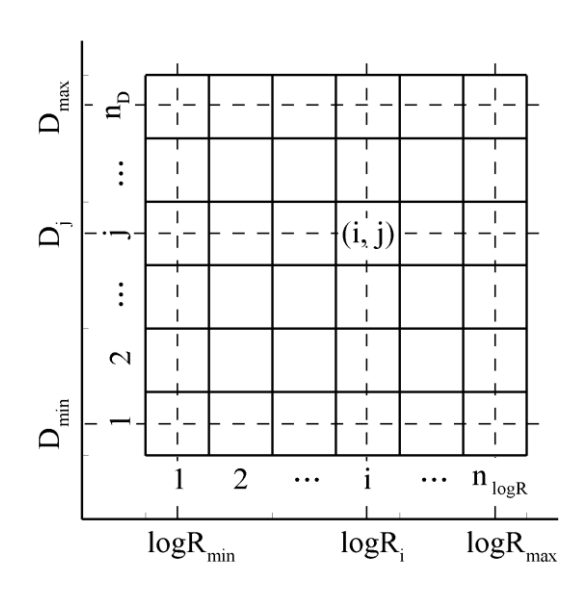


Figure 2. Discretization of log R and D at t = 0.

Model validation

To validate the model, we compare the predictions of QSM for single and polydisperse particles with experimental measurements of dissolution from polydisperse collections of felodipine drug particles in a Couette flow viscometer [23]. The molar volume of felodipine is $v_m = 265 \text{ cm}^3/\text{mol}$. The solubility of felodipine in density-matched water in the experiment is $C_{sol} = 0.89 \mu\text{M}$, which is also the saturation concentration (C_s). The diffusion coefficient of felodipine is $D_m = 6.7 \times 10^{-6} \text{ cm}^2/\text{s}$.

In the experiment, the particle shapes are random and irregular, and the initial particle size distribution roughly follows a log-normal distribution as shown in Fig. 3. The radius at the peak in the log-normal distribution is $R^* = 1.4 \mu m$. The maximum and minimum particle radii are $R_{min} = 0.47 \mu m$ and $R_{max} = 5.2 \mu m$, respectively. Since the size distribution is given as the volume fraction of each bin against particle radius in [23], we calculated the number of particles in each bin directly from a prespecified total volume of particles. A simple laminar shear flow with closely linear velocity profile was created by rotating the inner cylinder of the Couette viscometer at 5 rpm, generating a low Reynolds number laminar flow that, together with the small size of particles, produced highly diffusion-dominated dissolution from particles with random geometries.

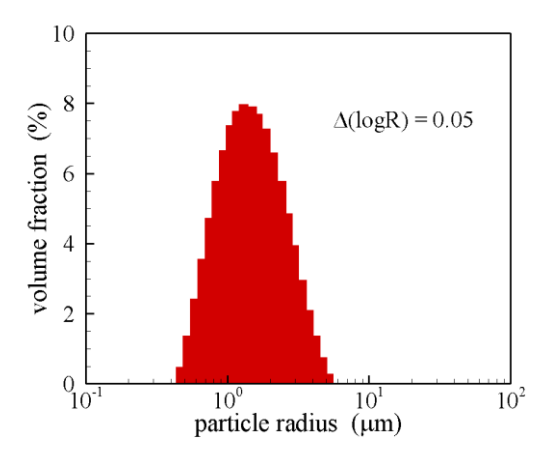


Figure 3 Initial particle size distribution measured with the Mastersizer instrument from in vitro experiment [23].

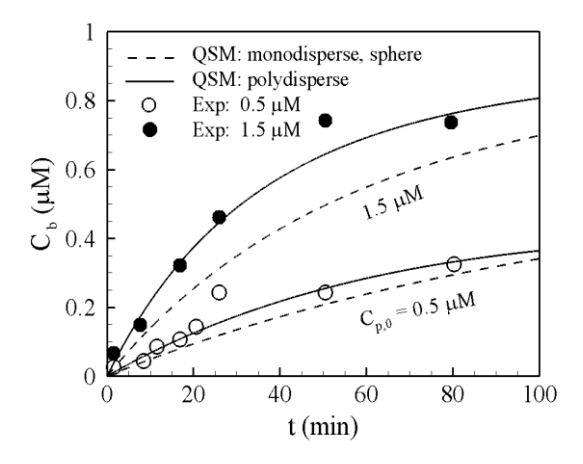


Figure 4. Predictions of the dissolution process using the monodisperse and polydisperse models, compared with experimental results [23].

In Fig. 4, we compare the prediction of the time variation of bulk concentration C_b from QSM for both monodisperse and polydisperse models with the experimental measurements. Two initial particle concentrations are considered, $C_{p0} = 0.5$ and 1.5 μ M. In the monodisperse model, the particles are assumed to be spherical and the particle radius is equal to R^* in the log-normal distribution in the experiment. In the polydisperse model, the particles are assumed to be spheroidal, with Taylor shape factor D from -9/11 to 9/11, corresponding to aspect ratio from 1/10 to 10. The initial PDF of particle size and shape, $P_{logR,D,0}^{\nu}$, follows the same distribution on logR as the experiment and is uniform over D. Overall, the predictions of the QSM are in good agreement with the experimental measurements. Comparison of the variation of C_b shows that the polydisperse model gives a better prediction than monodisperse model at every time point, because the particle size and shape distributions in the polydisperse model are closer to those of the particles in the experiment. The good agreement of the prediction of the polydisperse model with experimental measurements suggests that the polydisperse model can give accurate predictions of the dissolution process of complex systems with distributions of particle size and shape.

3. Examples of Polydisperse Dissolution

Here we select several typical cases of polydisperse dissolution of felodipine to demonstrate the ability of the model to predict dissolution process. We assume that at t = 0, the volumetric PDF $P_{logR,D,0}^{v}$ follows

the log-normal distribution with respect to logR for any D and is uniform over D from D_{min} to D_{max} for any logR, as described by Eqn. (35). The Taylor shape factor D ranges from -9/11 to 9/11, corresponding to aspect ratio from 1/10 (Prolate) to 10 (Oblate). The variance of the log-normal distribution $\sigma^2 = 0.18$. The minimum and maximum particle sizes are selected so as to make

$$(P_{logR,D,0}^{v})_{R=R_{0,min}} / (P_{logR,D,0}^{v})_{R=R^{*}} = (P_{logR,D,0}^{v})_{R=R_{0,max}} / (P_{logR,0}^{v})_{R=R^{*}} = 0.01$$
 (40)

Here $R_{0,min}$ and $R_{0,max}$ are the minimum and maximum particle radii at t=0, respectively. It can be calculated that

$$R_{0,min}/R^* = 0.28$$
 and $R_{0,max}/R^* = 3.62$ (41)

Figure 5 shows the initial profile of $P_{logR,0}^{v}$, which is the integral of $P_{logR,D,0}^{v}$ over D. The distribution is symmetric about $logR^*$.

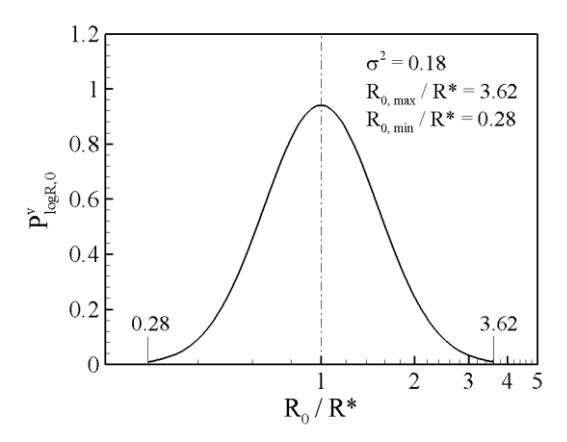


Figure 5. Initial particle size distribution $P_{logR,0}^{v}$ with respect to R_0/R^* .

In addition to particle size and shape, another factor determining the dissolution process is the initial solid particle concentration $C_{p,0}$. When $C_{p,0} < C_s$, all particles will completely dissolve in the solution. When $C_{p,0} = C_s$, all particles will completely dissolve and the solution will be saturated. When $C_{p,0} > C_s$, the particles will partially dissolve and the solution will be saturated.

We start with case of $C_{p,0}/C_s = 0.1$. Figure 6 shows the variation of typical particle sizes with time for $C_{p,0}/C_s = 0.1$. Overall, the particle sizes all decrease following a similar pattern. For the same initial size, the radius reduction rate, $|d(R/R^*)/d(t/\tau_{diss})|$, of non-spherical particles (D = -9/11 and 9/11) is larger than that of spherical particles (D = 0). This has been discussed in Wang et al. [28]. For any given particle, the reduction rate, $|d(R/R^*)/d(t/\tau_{diss})|$, increases with decrease in (R/R^*) , and approaches infinity when (R/R^*) goes to 0. For the same particle shape, that is, the same D, the reduction rate of smaller particles is larger than that of larger particles at the same t/τ_{diss} . These two phenomena are related to the dependence of particle size reduction rate on particle radius [25].

In Fig. 7 we plot the evolutions of volumetric PDF, $P_{logR,D}^{v}$, in the space of $log(R/R^*)$ and D. When $t/\tau_{diss} = 0$, the domain of particles is rectangular. $P_{logR,D}^{v}$ follows a log-normal distribution in the direction of $log(R/R^*)$ and remains constant in the direction of D. Due to particle size reduction, the domain of the distributions moves toward the left. In this process, the patterns of the distributions change

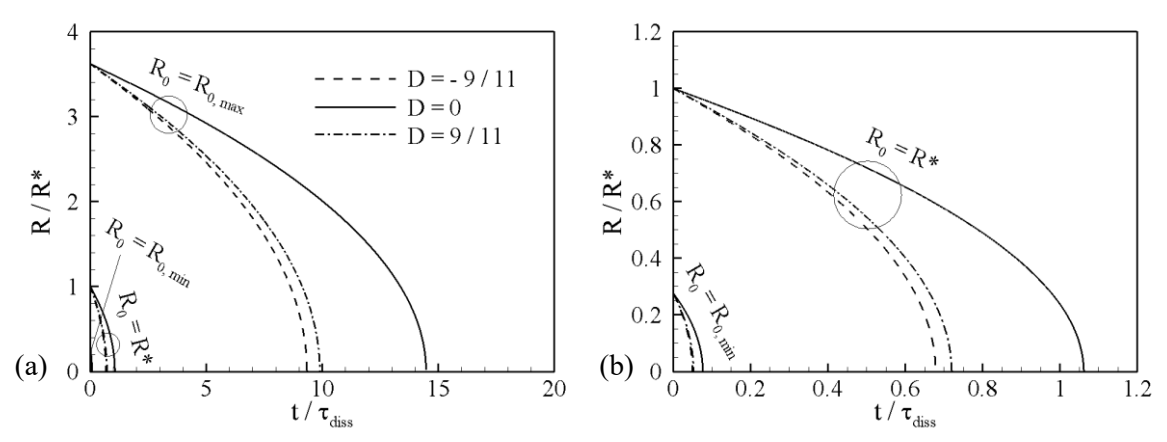


Figure 6. Variation of typical particle sizes with time for $C_{p,0}/C_s = 0.1$. (a) All three cases with $R_0 = R_{0,max}$, R^* , and $R_{0,min}$, (b) cases with $R_0 = R^*$, and $R_{0,min}$.

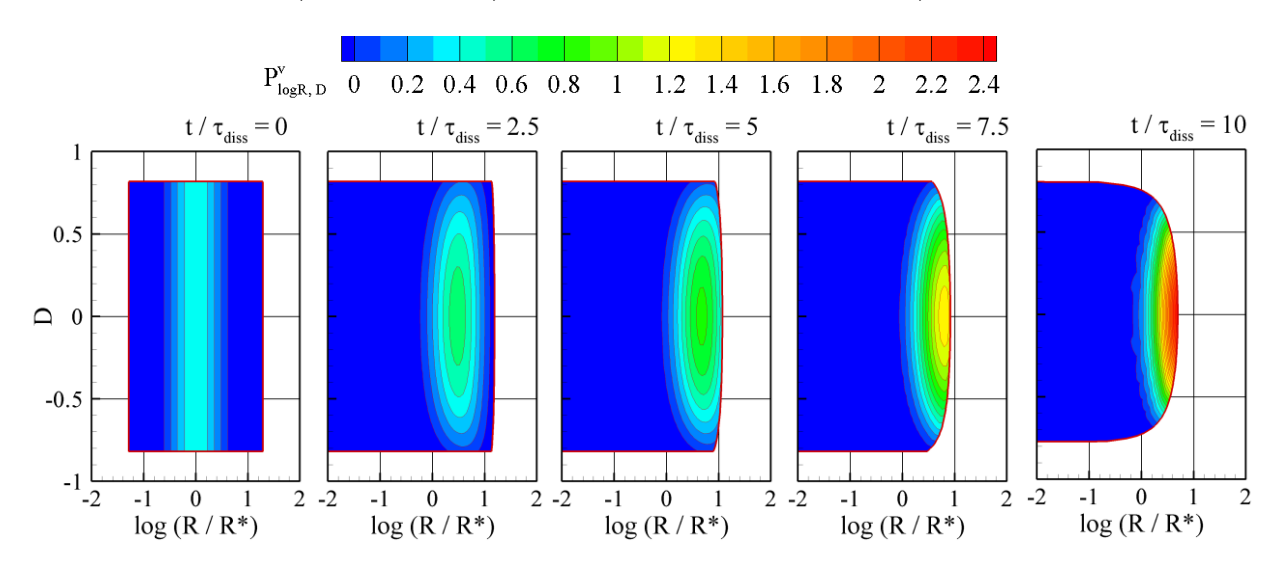


Figure 7. Evolution of particle size distribution $(P_{logR,D}^{v})$ in the space of $log(R/R^{*})$ and D for $C_{p,0}/C_{s} = 0.1$.

within the domain. Because of the larger size reduction rates of particles of larger |D|, $P^{\nu}_{logR,D}$, decreases in the upper and lower regions and converges to the central region where |D| is small. The non-uniform particle size reduction rate caused by the non-uniform distribution of D creates an arc curving to the left on the right boundary of the domain. At the same time, the faster size reduction rates of smaller particles cause the peak in the distribution of $P^{\nu}_{logR,D}$ to shift to the right, where it eventually reaches the right boundary.

For the $C_{p,0}/C_s=1$ cases, complete dissolution requires infinite time. The calculation was stopped at $C_b/C_s=0.99$. Figure 8 shows the variation of typical particle sizes with time for $C_{p,0}/C_s=1$. For all Taylor shape parameters, smaller particles, such as those with $R_0=R^*$ and $R_{0,min}$, completely dissolve within a finite range of time, yet the complete dissolution of the largest particles ($R_0=R_{0,max}$) cannot be achieved with a finite time.

Figure 9 shows the evolution of $P_{logR,D}^{\nu}$ over the time period from $t/\tau_{diss}=0$ to 100 for $C_{p,0}/C_s=1$. When $t/\tau_{diss}=100$, $C_b/C_s=0.99$ is roughly reached. The non-uniform particle size reduction makes

 $P_{logR,D}^{v}$ converge to the central region and move to the large particle side. At $t/\tau_{diss} = 100$, about 1% of the particle volume is left in the system, and the peak still has not reached the largest particles.

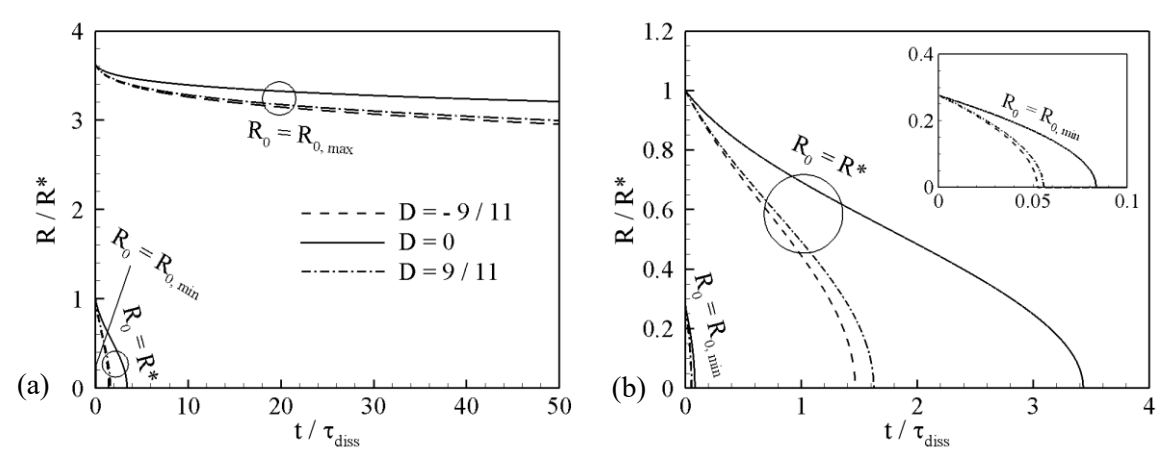


Figure 8. Variation of typical particle sizes with time for $C_{p,0}/C_s = 1$. (a) All three cases with $R_0 = R_{0,max}$, R^* , and $R_{0,min}$, (b) cases with $R_0 = R^*$, and $R_{0,min}$.

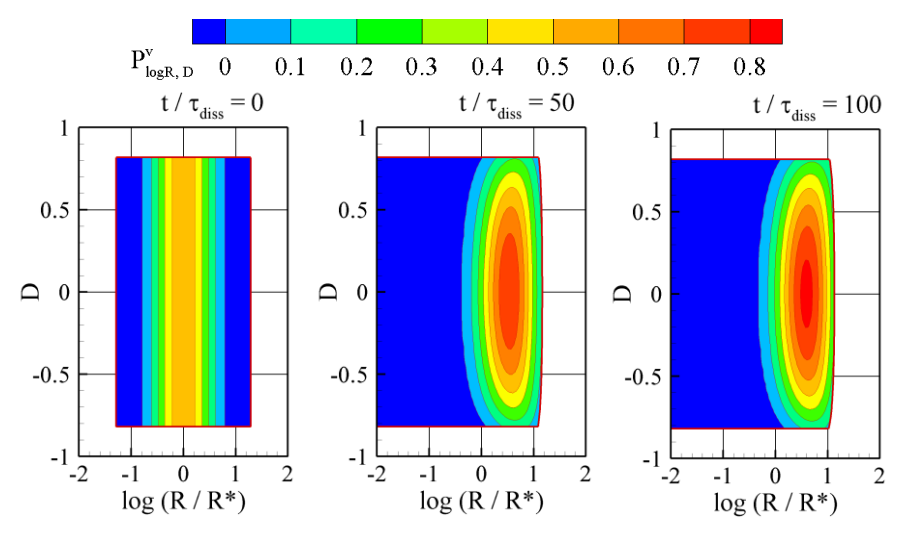


Figure 9. Evolution of particle size distribution $(P_{logR,D}^{v})$ in the space of log(R/R*) and D for $C_{p,0}/C_{s}=1$.

When $C_{p,0}/C_s = 10$, only 10% of the particle volume is dissolved in the solution when the process is complete, and the smaller particles play a more important role in the dissolution process. In Fig. 10, we plot the variation of typical particle sizes for $C_{p,0}/C_s = 10$. Similar to the cases of $C_{p,0}/C_s = 1$, it takes an infinite amount of time to reach full saturation, so the calculations were stopped when $C_b/C_s = 0.99$. In this case, the size of most particles decreases only slightly. Even the smallest particles do not completely dissolve. All particles asymptotically approach their respective final-state constant particle sizes.

Figure 11 shows the evolution of $P_{logR,D}^{v}$ for $C_{p,0}/C_s = 10$. When $t/\tau_{diss} = 0.2$, $C_b/C_s \approx 0.98$. As shown in the figure, the left boundary of the domain moves to the left, with larger extensions near the upper and bottom ends, due to the larger size reduction rates of particles of larger |D|. During the whole process, the distribution of $P_{logR,D}^{v}$ converges only slightly to the central region.

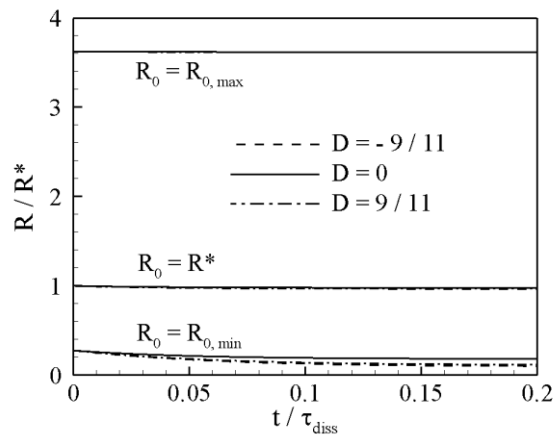


Figure 10. Variation of typical particle sizes with time for $C_{p,0}/C_s = 10$

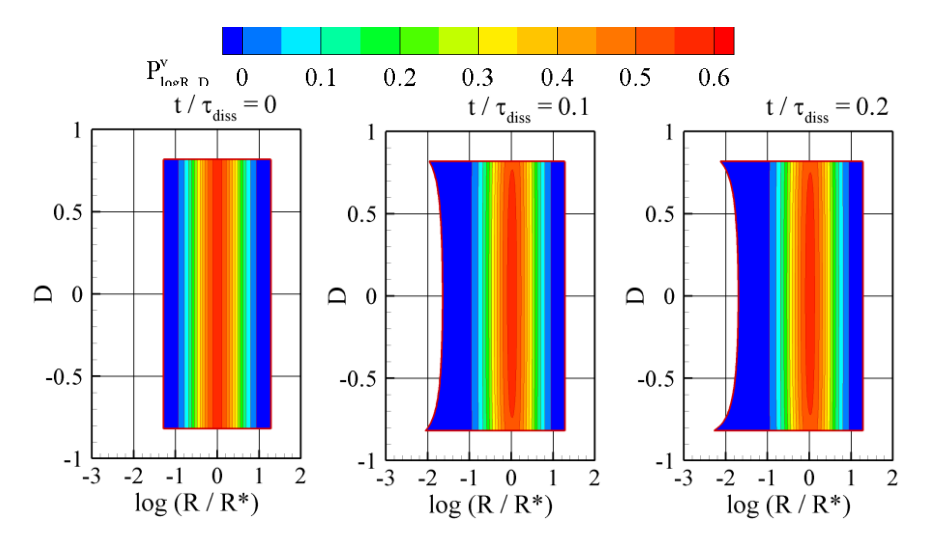


Figure 11. Evolution of particle size distribution $(P_{logR,D}^v)$ in the space of $log(R/R^*)$ and D for $C_{n,0}/C_s = 10$.

In Fig. 12 we compare the increase in bulk concentration $(C_{b,0}/C_s)$ of a polydisperse system with those of monodisperse systems for $C_{p,0}/C_s = 0.1$, 1, and 10. The Taylor shape parameters in the three monodisperse systems are D = -9/11, 0, and 9/11, respectively. When $C_{p,0}/C_s = 0.1$ and 1, the faster dissolution of smaller particles and particles of large |D| in polydisperse systems makes C_b/C_s increase in the initial short time period $(t/\tau_{diss} < 0.2)$ at a rate close to that in monodisperse systems with D = -9/11 and 9/11. It's a coincidence that the increase rate of polydisperse systems is close to that of monodisperse systems. When we widen or narrow the initial distributions of the polydisperse particles, they will not be close to each other.

After the initial time period, the larger particles play a more important role, which significantly reduces the dissolution rate. As a result, the increase of C_b/C_s in polydisperse systems becomes slower than in any of the monodisperse systems. Correspondingly, the dissolution time in polydisperse systems becomes much longer than in monodisperse systems. If a further wider initial distribution is used, the bulk concentration will increase faster than in the current polydisperse system in the initial period and increase slower after that. When $C_{p,0}/C_s = 10$, the dissolution process is dominated by smaller particles in the polydisperse system, and the smaller particles have a larger dissolution rate. As a result, the bulk concentration increases

at a rate close to that of monodisperse systems with D = -9/11 and 9/11. If the initial size distribution is further widened, C_b/C_s will increase even faster in the polydisperse system.

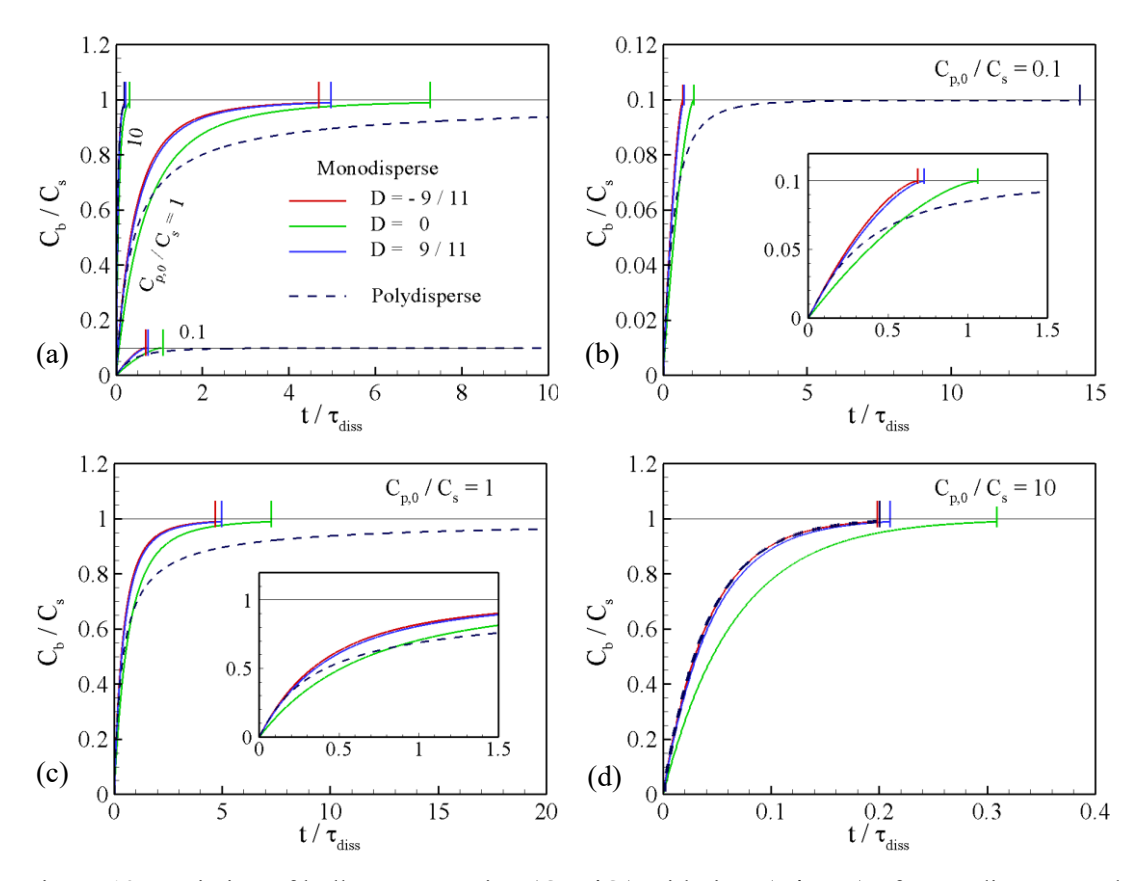


Figure 12. Variation of bulk concentration $(C_{p,0}/C_s)$ with time (t/τ_{diss}) of monodisperse and polydisperse particles. (a) Three initial particle concentrations, $C_{p,0}/C_s = 0.1$, 1 and 10, (b) $C_{p,0}/C_s = 0.1$, (c) $C_{p,0}/C_s = 1$, (d) $C_{p,0}/C_s = 10$.

4. Conclusion

In this paper, we have integrated a rigorous mathematically based quasi-steady-state model of diffusion-dominated dissolution of single spheroidal (prolate, oblate, or spherical) particles into the well-established framework of polydisperse dissolution models based on the assumption of uniform bulk concentration, and developed a mathematical model that can accurately predict the detailed dissolution process of systems of spheroidal particles with a broad range of distributions of particle size and aspect ratio. Validation against experimental results show that this model can accurately predict the increase in bulk concentration of complex polydisperse systems with various particle sizes and shapes. Several examples of the polydisperse dissolution of felodipine particles have been utilized to demonstrate the model's capability to predict the intricate and detailed dissolution process.

This model lays an important foundation for the future development of mathematical models of the dissolution of irregularly shaped polydisperse particle systems in practical applications.

Data accessibility. The data that support the findings of this study are available from the corresponding author upon reasonable request.

Competing interests. We declare that we have no competing interests.

Funding. This work was supported by the National Science Foundation (Award ID: 2138740)

References

- [1] Salehi, N., Al-Gousous, J., Mudie, D.M., Amidon, G.L., Ziff, R.M. & Amidon, G.E. 2020 Hierarchical mass transfer analysis of drug particle dissolution, highlighting the hydrodynamics, pH, particle size, and buffer effects for the dissolution of ionizable and nonionizable drugs in a compendial dissolution vessel. *Molecular Pharmaceutics* **17**, 3870-3884.
- [2] Petersen, J. 2016 Heap leaching as a key technology for recovery of values from low-grade ores—A brief overview. *Hydrometallurgy* **165**, 206-212.
- [3] Badgujar, K.C. & Bhanage, B.M. 2015 Factors governing dissolution process of lignocellulosic biomass in ionic liquid: Current status, overview and challenges. *Bioresource technology* **178**, 2-18.
- [4] Chamolly, A. & Lauga, E. 2019 Stochastic dynamics of dissolving active particles. *The European Physical Journal E* **42**, 1-15.
- [5] Sheng, J.J., Sirois, P.J., Dressman, J.B. & Amidon, G.L. 2008 Particle diffusional layer thickness in a USP dissolution apparatus II: a combined function of particle size and paddle speed. *Journal of Pharmaceutical Sciences* **97**, 4815-4829.
- [6] Hörter, D. & Dressman, J. 2001 Influence of physicochemical properties on dissolution of drugs in the gastrointestinal tract. *Advanced drug delivery reviews* **46**, 75-87.
- [7] Jambhekar, S.S. & Breen, P.J. 2013 Drug dissolution: significance of physicochemical properties and physiological conditions. *Drug Discovery Today* **18**, 1173-1184.
- [8] Wang, Y. & Brasseur, J.G. 2019 Enhancement of mass transfer from particles by local shear-rate and correlations with application to drug dissolution. *AIChE Journal* **65**, e16617.
- [9] Costa, P. & Lobo, J.M.S. 2001 Modeling and comparison of dissolution profiles. *European journal of pharmaceutical sciences* **13**, 123-133.
- [10] Simöes, S., de Almeida, L.P. & Figueiredo, M. 1996 Testing the applicability of classical diffusional models to polydisperse systems. *International journal of pharmaceutics* **139**, 169-176.
- [11] De Almeida, L.P., Simões, S., Brito, P., Portugal, A. & Figueiredo, M. 1997 Modeling dissolution of sparingly soluble multisized powders. *Journal of Pharmaceutical Sciences* **86**, 726-732.
- [12] Dali, M. 1999 Determination of mass transfer dissolution rate constants from critical time of dissolution of a powder sample. *Pharmaceutical development and technology* **4**, 1-8.
- [13] Wang, J. & Flanagan, D.R. 1999 General solution for diffusion-controlled dissolution of spherical particles. 1. Theory. *Journal of Pharmaceutical Sciences* **88**, 731-738.
- [14] Wang, J. & Flanagan, D.R. 2002 General solution for diffusion-controlled dissolution of spherical particles. 2. Evaluation of experimental data. *Journal of Pharmaceutical Sciences* **91**, 534-542.
- [15] Shan, G., Igarashi, K. & Ooshima, H. 2002 Dissolution kinetics of crystals in suspension and its application to L-aspartic acid crystals. *Chemical Engineering Journal* **88**, 53-58.
- [16] Hintz, R.J. & Johnson, K.C. 1989 The effect of particle size distribution on dissolution rate and oral absorption. *International journal of pharmaceutics* **51**, 9-17.

- [17] Lu, A.T., Frisella, M.E. & Johnson, K.C. 1993 Dissolution modeling: factors affecting the dissolution rates of polydisperse powders. *Pharmaceutical research* **10**, 1308-1314.
- [18] Johnson, K.C. 2003 Dissolution and absorption modeling: model expansion to simulate the effects of precipitation, water absorption, longitudinally changing intestinal permeability, and controlled release on drug absorption. *Drug development and industrial pharmacy* **29**, 833-842.
- [19] Johnson, K.C. 2012 Comparison of methods for predicting dissolution and the theoretical implications of particle-size-dependent solubility. *Journal of Pharmaceutical Sciences* **101**, 681-689.
- [20] Nielsen, A.E. 1961 Diffusion controlled growth of a moving sphere. The kinetics of crystal growth in potassium perchlorate precipitation. *The Journal of Physical Chemistry* **65**, 46-49.
- [21] Wang, Y., Abrahamsson, B., Lindfors, L. & Brasseur, J.G. 2012 Comparison and analysis of theoretical models for diffusion-controlled dissolution. *Molecular Pharmaceutics* **9**, 1052-1066.
- [22] Higuchi, W. & Hiestand, E. 1963 Dissolution rates of finely divided drug powders I. Effect of a distribution of particle sizes in a diffusion-controlled process. *Journal of Pharmaceutical Sciences* **52**, 67-71.
- [23] Lindfors, L., Jonsson, M., Weibull, E., Brasseur, J.G. & Abrahamsson, B. 2015 Hydrodynamic effects on drug dissolution and deaggregation in the small intestine—a study with felodipine as a model drug. *Journal of Pharmaceutical Sciences* **104**, 2969-2976.
- [24] Wu, D., Tsekouras, A.A., Macheras, P. & Kesisoglou, F. 2023 Physiologically based pharmacokinetic models under the prism of the finite absorption time concept. *Pharmaceutical research* **40**, 419-429.
- [25] Wang, Y., Abrahamsson, B., Lindfors, L. & Brasseur, J.G. 2015 Analysis of Diffusion-Controlled Dissolution from Polydisperse Collections of Drug Particles with an Assessed Mathematical Model. *Journal of Pharmaceutical Sciences* **104**, 2998-3017. (doi:https://doi.org/10.1002/jps.24472).
- [26] Zhong, W., Yu, A., Zhou, G., Xie, J. & Zhang, H. 2016 CFD simulation of dense particulate reaction system: Approaches, recent advances and applications. *Chemical Engineering Science* **140**, 16-43.
- [27] Zhong, W., Yu, A., Liu, X., Tong, Z. & Zhang, H. 2016 DEM/CFD-DEM modelling of non-spherical particulate systems: theoretical developments and applications. *Powder technology* **302**, 108-152.
- [28] Wang, Y., Wan, H., Wei, T., Nevares, D. & Shu, F. 2022 Quasi-steady-state modelling and characterization of diffusion-controlled dissolution from monodisperse prolate and oblate spheroidal particles. *Proceedings of the Royal Society A* **478**, 20220283.
- [29] Noyes, A.A. & Whitney, W.R. 1897 The rate of solution of solid substances in their own solutions. *Journal of the American chemical society* **19**, 930-934.
- [30] Wang, Y., Vazquez Alvarez, D., Wan, H., Gonzalez Pizarro, R. & Shu, F. 2023 Advection-enhanced heat and mass transport from neutrally suspended droplet in simple shear flow. *Physics of Fluids* **35**.
- [31] LeBlanc, S. & Fogler, H.S. 1987 Population balance modeling of the dissolution of polydisperse solids: rate limiting regimes. *AIChE journal* **33**, 54-63.
- [32] Randolph, A. 2012 Theory of particulate processes: analysis and techniques of continuous crystallization, Elsevier.
- [33] Gokhale, Y., Kumar, J., Hintz, W., Warnecke, G. & Tomas, J. 2008 Population Balance Modelling for Agglomeration and Disintegration of Nanoparticles. *Micro-Macro-interaction: In Structured media and Particle Systems*, 299-309.
- [34] Heintzenberg, J. 1994 Properties of the log-normal particle size distribution. *Aerosol Science and Technology* **21**, 46-48.
- [35] Bergmann, R.B., Shi, F.G., Queisser, H.J. & Krinke, J. 1998 Formation of polycrystalline silicon with lognormal grain size distribution. *Applied surface science* **123**, 376-380.